A fossil coral perspective on western tropical Pacific climate ~350 ka

K. Halimeda Kilbourne and Terrence M. Quinn
College of Marine Sciences, University of South Florida, St. Petersburg, Florida, USA

Frederick W. Taylor
Institute for Geophysics, University of Texas at Austin, Austin, Texas, USA

Received 26 June 2003; revised 16 December 2003; accepted 13 January 2004; published 5 March 2004.

[1] The nature of tropical climate variability ~350 ka is addressed using $\delta^{18}O$ and Sr/Ca records from a modern and a fossil coral from Vanuatu (southwestern tropical Pacific Ocean). Modern El Niño events at Vanuatu produce positive coral $\delta^{18}O$ and Sr/Ca anomalies; similar anomalies observed in the fossil coral records suggest that El Niño was operative 350 kyr ago. Seasonal variations in coral Sr/Ca, a sea surface temperature (SST) proxy, have the same amplitude in both corals, whereas seasonal $\delta^{18}O$ variations are smaller in the fossil coral than in the modern coral. This is consistent with displacement of the South Pacific Convergence Zone toward the southwest during the boreal summer ~350 ka. Mathematical modeling results preclude warmer SST and higher SSS at Vanuatu during this time, but permit the surface ocean to be ~2°C cooler and 0–2 psu fresher than today. Assessing the potential of variations in late Quaternary seawater Sr/Ca remains the largest obstacle to accurately reconstructing tropical SST using pristine fossil corals. *INDEX TERMS:* 4215 Oceanography: General: Climate and interannual variability (3309); 4267 Oceanography: General: Paleoceanography; 4870 Oceanography: Biological and Chemical: Stable isotopes; 1065 Geochemistry: Trace elements (3670); 4522 Oceanography: Physical: El Nino; 4275 Oceanography: General: Remote sensing and electromagnetic processes (0689); *KEYWORDS:* coral, climate, geochemistry

Citation: Kilbourne, K. H., T. M. Quinn, and F. W. Taylor (2004), A fossil coral perspective on western tropical Pacific climate ~350 ka, *Paleoceanography*, *19*, PA1019, doi:10.1029/2003PA000944.

1. Introduction

[2] The El Niño-Southern Oscillation (ENSO) dominates interannual variations in the tropical climate system. Intensive investigations for over 20 years concerning the ENSO phenomenon have yielded significant insights into the coupled ocean-atmosphere dynamics that give rise to this mode of climate variability in the modern and in the recent past. Computer simulations of ENSO [*Zebiak and Cane*, 1987; *Suarez and Schopf*, 1988; *Battisti and Hirst*, 1989] indicate that the amplitude, frequency, and regularity of ENSO events are sensitive to climate-related model parameters, suggesting that interannual variability is sensitive to background climate state [*Enfield and Cid*, 1991]. A change in the frequency and intensity of El Niño events since the "climate regime shift" of the mid-1970s illustrates the possibility of a nonstationary ENSO system [*Quinn and Neal*, 1984, 1985; *Nitta and Yamada*, 1989; *Trenberth and Hurrel*, 1994; *Minobe*, 1997, 1999; *An and Wang*, 2000; *Fedorov and Philander*, 2000; *Stephens et al.*, 2001; *Wang and An*, 2001].

[3] Evaluating modulations in ENSO during different background climate states requires records of El Niño events from times of different background climate. Instrumental records that could be used to reconstruct ENSO, such as sea surface temperature (SST) or SST anomalies (SSTA) in the eastern equatorial Pacific Ocean and the Southern Oscillation Index, do not extend much further back in time than the end of the 19th century, if that far. Instrumental SSTA records of ENSO are more complete both spatially and temporally post 1950. Instrumental sea surface salinity (SSS) records of ENSO are extremely rare and the ones that exist extend back only to the 1970s [e.g., *Lagerloef and Delcroix*, 1999; *Gouriou and Delcroix*, 2002].

[4] The possibility of nonstationary behavior of the ENSO system has lead to a series of studies investigating changes in ENSO during the Pleistocene and early Holocene [e.g., *Clement et al.*, 1999; *Hughen et al.*, 1999; *McCulloch et al.*, 1999; *Rittenour et al.*, 2000; *Tudhope et al.*, 2001; *Kukla et al.*, 2002]. Some initial findings from sediment cores and fossil mollusks from archaeological sites indicate that interannual ENSO variability is a phenomenon of the middle to late Holocene, but did not exist in the Late Pleistocene [*Sandweiss et al.*, 1996; *Rodbell et al.*, 1999]. However, data from fossil corals appear to indicate that ENSO variations during interglacial periods were similar to recent (19th and 20th century) variations [*Hughen et al.*, 1999] and that ENSO was weaker but still active during glacial periods [*Tudhope et al.*, 2001]. *Tudhope et al.* [2001] show that ENSO has existed back at least 130 ± 2 kyr.

[5] The mechanisms driving ENSO variability on geologic timescales are still enigmatic [*Clement et al.*, 1999]. Coupled ocean-atmosphere general circulation models have been used to investigate some of the possible processes involved. Climate modeling indicates that the precessional cycle of insolation can interact with zonal asymmetry in Pacific SST and cause an increased frequency of warm (cool) events when there is an anomalous cooling (warming) in the late summer/fall [*Clement et al.*, 1999]. Another similar model

0883-8305/04/2003PA000944$12.00

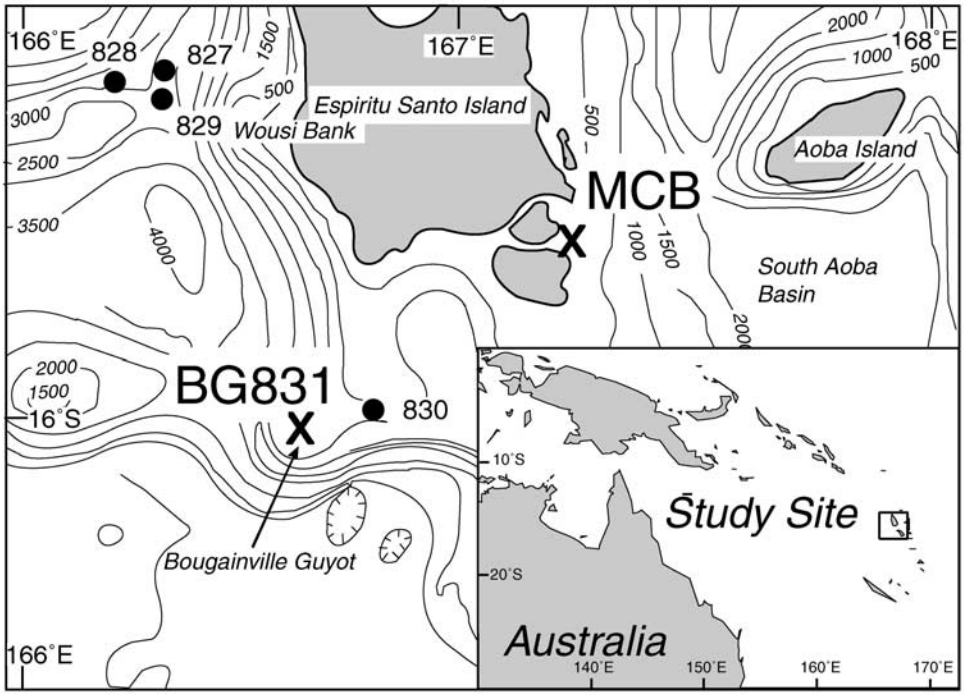

Figure 1. Locations ("X") of modern (Malo Channel (MCB), Espiritu Santo Island, Republic of Vanuatu) and fossil (BG831; Bougainville Guyot, ODP Site 831) coral sampling sites. The inset map of southwest Pacific basin shows the larger geographic context.

indicates that an increase in warm events during early glaciation may induce high-latitude ice buildup [*Kukla et al.*, 2002]. The paleoclimate data that exist are insufficient to adequately verify model results, and more data are needed.

[6] Proxy climate records (e.g., tree rings, ice cores, and corals; *Dunbar and Cole* [1999] for an overview) are required to investigate changes in ENSO in the preinstrumental period. Proxy records that overlap with, and extend beyond, the instrumental period offer a unique perspective on ENSO variability and can be used to address tropical climate variability on submillennial timescales. Proxy climate records also provide a data set from the tropical oceans that can be used to test model output and to provide constraints on climate model input.

[7] Corals are ideal for reconstructing seasonal to interannual variations in the tropical surface oceans because they are long-lived (many survive for centuries), their skeletons have annual density bands that provide chronological control and subannual resolution, they are widely distributed, and their skeletons are amenable to geochemical analyses. Two of the most widely used geochemical determinations of coral aragonite are stable oxygen isotope ratios and Sr/Ca ratios. Coral oxygen isotopic ratios ($\delta^{18}O$) reflect both temperature and the oxygen isotopic composition of the seawater ($\delta^{18}O_{sw}$) at the time of carbonate precipitation [e.g., *Epstein et al.*, 1953; *Goreau*, 1977; *Weber and Woodhead*, 1972; *McConnaughey*, 1989; *Fairbanks et al.*, 1997]. $\delta^{18}O_{sw}$ in the modern ocean responds to salinity changes brought about by evaporation or precipitation and, in coastal zones, by fluvial input [*Craig and Gordon*, 1965; *Bigg and Rohling*, 2000]. Sr/Ca ratios in the modern ocean are largely invariant and the Sr/Ca ratios in corals vary in response to changes in surface ocean temperature [e.g., *Beck et al.*, 1992]. Paired analyses of Sr/Ca and $\delta^{18}O$ on a single coral sample can result in the unique solution of SST and SSS [*McCulloch et al.*, 1996; *Gagan et al.*, 1998; *Ren et al.*, 2003].

[8] Here we present $\delta^{18}O$ and Sr/Ca data from an exceptionally preserved fossil coral recovered from Bougainville Guyot (16°00.56′S, 166°40.34′E), located near Espiritu Santo Island in the Republic of Vanuatu (Figure 1). The fossil coral is ~350 kyr old, an age that places the most likely time of coral growth during a time when sea level was lower than today; possibly during Marine Isotope Stage (MIS) 10. In this study, we compare geochemical variations in the fossil coral with those from a modern coral from near Espiritu Santo Island (15.7S, 167.2E; Figure 1) to address two fundamental questions:

[9] 1. What was the background climate state of the tropical Pacific ~350 kyr ago, in terms of sea surface temperature (SST) and sea surface salinity (SSS)?

[10] 2. Is there evidence of ENSO activity at ~350 ka?

2. Ocean-Atmospheric Interactions in the Western Pacific

[11] Ocean conditions in the western tropical Pacific both respond to and force atmospheric phenomena. The Western Pacific Warm Pool (WPWP) is the largest oceanic heat source in the world and strongly affects global climate on a variety of timescales, especially interannually (ENSO). Ocean-atmosphere interactions in the Vanuatu region of the South Pacific are dominated by spatial and temporal

variability in the linkages between warm SST associated with the WPWP and atmospheric convection associated with the South Pacific Convergence Zone (SPCZ).

[12] The SPCZ is a zone of atmospheric convergence of the trade winds, and can be thought of as an extension of the Intertropical Convergence Zone (ITCZ) that stretches roughly from Papua New Guinea east to 120°W, 30°S [*Vincent*, 1994]. The spatial extent of the SPCZ changes in response to changing wind fields and SST on seasonal, interannual, and multidecadal timescales. The SPCZ is stronger in the austral summer than in the austral winter. Summertime warm SSTs facilitate upward convection in the atmosphere and northeasterly trade winds merge into the southeasterly trades along the SPCZ [*Vincent*, 1994]. The combination of warm SSTs and atmospheric convergence are associated with low atmospheric pressure and a persistent cloud band over the SPCZ. In the austral winter, the WPWP shifts to the north as Northern Hemisphere summer progresses. A shift in the wind field moves the focus of low-level tropospheric convergence to the ITCZ in the Northern Hemisphere during the austral winter [*Vincent*, 1994]. The locus of convection moves northward with the warm water and the winds, resulting in the SPCZs apparent northward movement into the ITCZ.

[13] The strength and position of the SPCZ also varies on multidecadal timescales according to the phase of the Interdecadal Pacific Oscillation (IPO; a Pacific-wide manifestation of the Pacific Decadal Oscillation; *Folland et al.* [2002]). SPCZ movements in response to the phase of the IPO are quasi-independent of, but of the same magnitude as, SPCZ movements in response to ENSO [*Folland et al.*, 2002]. In general, a positive phase of the IPO is related to a northeast shift in the SPCZ (the case from 1977 to the present), and a negative phase of the IPO is related to a southwest shift in the SPCZ (the situation from the mid-1940s to the mid-1970s). These types of movements become important when interpreting a climate proxy record because the proxy has been recording a Eulerian measurement of a moving system. In other words, the corals remain in the same location but surface ocean currents and atmospheric phenomena may change their position with time.

3. Climatic Setting of Vanuatu

[14] Vanuatu is well situated to study changes in tropical climate variability because it is positioned beneath the SPCZ, along the southern edge of the WPWP, and it is affected by spatial and intensity variations in both. Thus ENSO forcing is strong at Vanuatu and surface-ocean conditions there reflect the influence of important climate forcing.

[15] Movements of the SPCZ and its associated salinity front control small seasonal SSS changes (0.36 average annual range 1980–1992; *Levitus and Boyer* [1994]) and larger interannual SSS changes (1.91 maximum range 1980–1992; *Gouriou and Delcroix* [2002]) in this region. The SPCZ lies to the northwest of Vanuatu during the austral winter and in the austral summer it moves southeast over Vanuatu, bringing with it enormous amounts of rain contributing to regionally lower SSS at that time [*Gouriou and Delcroix*, 2002]. During ENSO warm phase (cool phase) years, the SPCZ weakens (strengthens) and Vanuatu is dry (wet). Salinity increases sharply during a warm phase event due to a combination of more saline waters advecting from south of the SPCZ and an increase in the local evaporation to precipitation ratio [*Picaut et al.*, 1996, 1997, 2001; *Vialard and Delecluse*, 1998].

[16] The average SST for a $1° \times 1°$ grid box centered near Espiritu Santo Island, Vanuatu (hereafter Santo) at 166.5E and 15.5S is 27.7°C (1980–1992; *Levitus and Boyer* [1994]). This places Santo on the edge of the WPWP (as defined by 28°C mean annual SST contour), so it is affected by spatial and temporal changes in the warm pool. The average seasonal SST cycle near Santo, is 2.5°C [*Levitus and Boyer*, 1994], and the interannual SST variations are small relative to the seasonal cycle. SSTs generally decrease (increase) during ENSO warm phase (cool phase) years, as warm water from the warm pool advects toward the central Pacific.

[17] It is important to note that not all ENSO events manifest in exactly the same manner at Santo (Figure 2). There are some warm phase years where a small SSTA is associated with a strong sea surface salinity anomaly (SSSA; 1983), while other years have strong SSTA and weak SSSA (1987). Still other ''events'' last for multiple years, such as the mild El Niño of the early 1990s [*Trenberth and Hoar*, 1996, 1997]. The key to recognizing ENSO from temperature and salinity records in the Santo region is determining the sense and duration of the SSSA and SSTA.

[18] For the purpose of this study ENSO events must be defined in terms recognizable in a proxy record, faithful to the local modern instrument record, and consistent with conventional definitions. In a fashion similar to *Trenberth* [1997], the 5-month running mean of surface anomalies are used to define an ENSO event. We define an ENSO warm (cool) phase event at Santo (Figure 2) to be indicated by a simultaneous SSTA decrease (increase) and SSSA increase (decrease), of a magnitude greater than 1.5 standard deviations of the running mean for more than 6 months of either SSSA or SSTA ($\delta^{18}O$ or Sr/Ca anomalies in proxy situations).

[19] The definition above differs from that of *Trenberth* [1997] in two ways. Surface salinity anomalies are included in the definition in addition to SSTA because the local response to El Niño at Santo can be either strong salinity anomalies or strong temperature anomalies, and is often both. Another difference is the use of a fractional standard deviation threshold as opposed to a specific temperature (0.4°C) as in the work of *Trenberth* [1997]. The fractional standard deviation threshold captures anomalies that are proportionally large compared to the variance in the specific record. When considering records of past SSTA and SSSA that may have a smaller or larger amount of variance, the standard deviation threshold may be a more robust indicator of significant change relative to the mean.

4. Methods

4.1. Physical Sampling of Corals

[20] A living *Porites lutea* head was cored in 1.5 m of water within Malo Channel, which is located between Malo

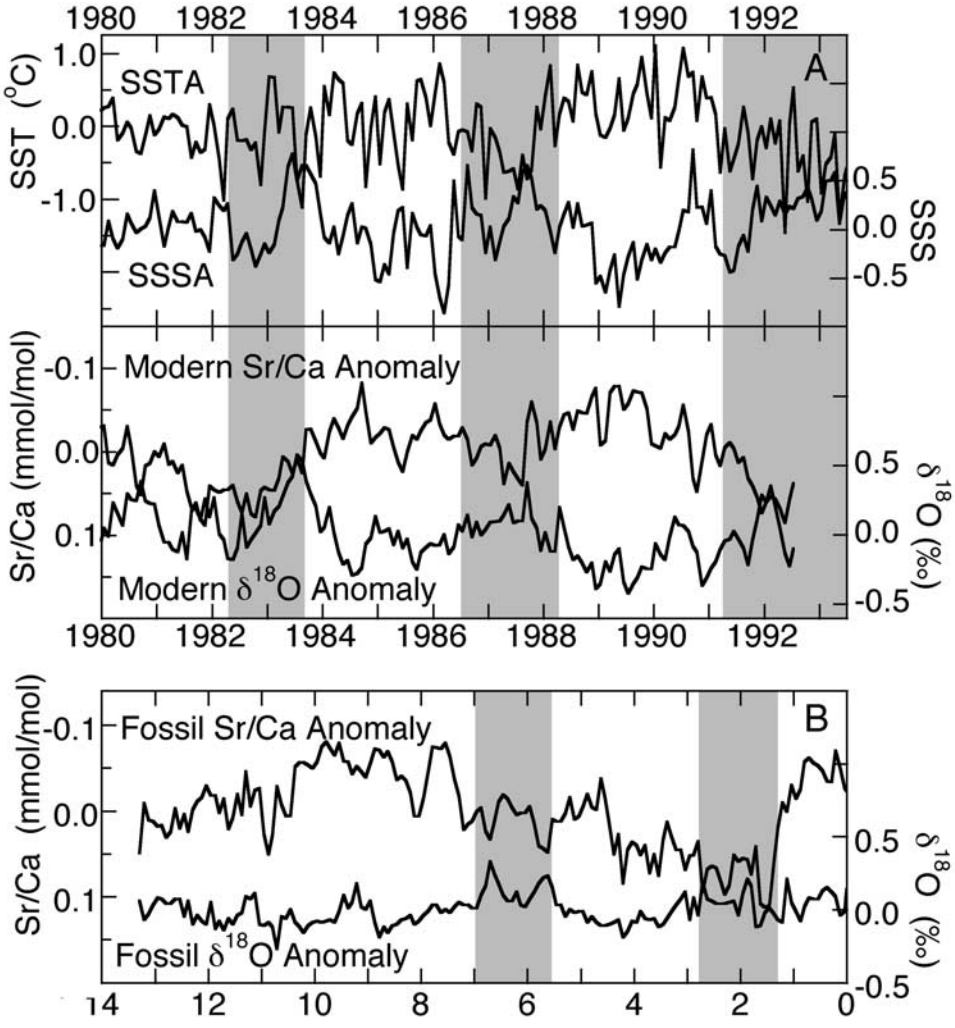

Figure 2. Comparison between instrumental and coral proxy records of climate variability at Espiritu Santo Island, Vanuatu. (a) Monthly SSTA [*Parker et al.*, 1995] and SSSA [*Gouriou and Delcroix*, 2002] are shown above, and modern coral monthly Sr/Ca anomaly and $\delta^{18}O$ anomaly are shown below. Anomalies are calculated as deviations from the monthly climatological average calculated from 1980 to 1992. Gray bars in the top graph represent ENSO warm phase events as defined by *Trenberth* [1997]. (b) Pleistocene coral Sr/Ca and $\delta^{18}O$ anomalies from fossil coral sample BG831. Grey bars in Figure 2b denote Pleistocene ENSO warm phase events, applying the criteria defined for the modern relationship between coral proxy records and instrumental records.

Island and Espiritu Santo Island in the Republic of Vanuatu (Figure 1) in 1992. The site was chosen because of its exposure to open-ocean conditions, minimizing any local microclimate effects. A 5 mm-wide slab was removed from the core (henceforth referred to as MCB) and subjected to X-radiography, revealing density band couplets. The slab is composed of 8 individual pieces, which fit together well, thereby ensuring stratigraphic completeness. Samples of the coral slab were removed as powder using a computer controlled drilling stage and drill mount. Powder samples were generated by routing a 3 mm wide swath, ~1 mm deep and collecting the powder every 1.33 mm down the slab.

[21] The fossil *Porites sp.* sample was recovered from the carbonate sequence of Bougainville Guyot during ODP Leg 134 at Site 831B in 1992 (831B-18R-1, 110–125; *Taylor et al.*, 1994). The sample (henceforth referred to as BG831) is 15 cm long and was recovered from 238.3 m below the seafloor in 1066 m of water. Similarly to the modern coral, BG831 was cut into a slab 5 mm wide, X-radiographed to reveal density bands, and drilled for aragonite powder. Because the fossil coral grew more slowly than the modern coral, individual samples from BG831 were extracted every 0.67 mm.

[22] Representative samples from the modern and fossil coral were subjected to a variety of tests to determine the preservation state of the fossil coral. Initially BG831 was subjected to X-ray diffractometry to test for the presence of calcite. A thin section of the same coral was examined

under a petrographic microscope and both MBC and BG831 were examined using scanning electron microscopy for evidence of secondary aragonite or calcite.

4.2. Age Determination of the Fossil Coral

[23] The age of the fossil coral sample was determined by a combination of radiometric (uranium series and Sr isotopes) and stratigraphic modeling techniques. The U-series determinations were performed at the University of Minnesota using thermal ionization mass spectrometry (TIMS) and the results have been previously published [*Taylor et al.*, 1994]. The Sr isotope determinations were performed at the University of Michigan radiogenic chemistry laboratory and the results have been previously published [*Quinn et al.*, 1994].

[24] Stratigraphic modeling was performed to calculate the elevation of the sample through time using the subsidence rate [*Taylor et al.*, 1994] and present-day depth of sample. The intersection of the sample elevation with Quaternary sea-level curves (SPECMAP Stack; *Imbrie et al.* [1984]; and sea level from *Shackleton* [2000]) dictates the sample age. Coral growth position errors of ±10 m were used in all of the calculations.

4.3. Stable Isotopes and Elemental Ratios

[25] Stable isotopic determinations were made on coral powder samples at the University of South Florida, College of Marine Science using a ThermoFinnigan Delta Plus XL dual-inlet mass spectrometer with an attached Kiel carbonate preparation device. Carbon and oxygen isotope data have a precision of 0.04 and 0.08‰, respectively (1σ), as calculated from repeated measurements of the standard NBS-19.

[26] Sr/Ca determinations were made on coral powder samples at the University of South Florida, College of Marine Science using a PerkinElmer Optima 4300DV dual-view ICP-OES, following the drift-correction methods of *Schrag* [1999]. Each coral sample (~250 mg) is dissolved in 10 mL of 2% (v/v) trace metal-grade nitric acid diluted with superdeionized water (resistance equals 18 MΩ). Gravimetric standards were made by combining Mg, Ca, Sr, U and Ba from SPEX ultrapure solution standards in proportions to match those of a typical coral. The accuracy of the Sr/Ca ratio of our gravimetric standards was confirmed via TIMS analysis at the University of Minnesota. Bulk coral powder from a modern *Porites lutea* sample from Santo was also dissolved in 2% (v/v) trace metal-grade nitric acid to make a ''coral standard'' solution. The coral standard solution was routinely analyzed as part of each run. Blanks of acid and deionized water are routinely monitored for contamination. Analytical precision (2σ) for Sr/Ca determinations used in this study is estimated to be 0.15% (0.013 mmol/mol), based on 86 determinations of the coral standard solution.

[27] Geochemical data were converted from the depth domain to the time domain by matching the maxima (minima) in Sr/Ca to minima (maxima) in SST data and linearly interpolating between, using the software package AnalySeries [*Paillard et al.*, 1996]. In the modern coral, SST data as extracted from a 1° by 1° grid box (GISST 2.3b; *Parker et al.* [1995]) was matched to the coral Sr/Ca. For BG831, the monthly climatological average SST served as a substitute for monthly SST data. Checking the age models visually against annual banding evident in the X-radiographs ensured accuracy of our depth to time conversions.

5. Results

5.1. Age of BG831

[28] Sample BG831 has a ^{230}Th age of 450 kyr ± 20, a ^{234}U/^{238}U age of 612 kyr ± 15 and an initial δ^{234}U value of 96 ± 7. The lack of concordance between the ^{230}Th and ^{234}U/^{238}U ages is probably caused by leakage of ^{234}U related to alpha-recoil processes [*Edwards et al.*, 1991]. Alpha-recoil processes would yield calculated ages that are older than true ages so that the calculated ages of sample BG831 should be considered maximum ages [*Taylor et al.*, 1994]. The initial δ^{234}U value of 96 ± 7 for BG831 is substantially lower than the initial δ^{234}U values modern coral samples (~150 ± 10; *Edwards et al.* [1986]; *Bar-Matthews et al.* [1993]; *Henderson et al.* [1993]) and is indicative of open-system behavior with respect to uranium, but not necessarily other elements within the aragonite crystalline structure (i.e., uranium can exhibit open-system behavior and strontium can exhibit closed-system behavior; *Bar-Matthews et al.* [1993]).

[29] Additional coral samples constrain the age of sample BG831 to be younger than ~370 kyr. A coral sample (831B-18R-2, 44–46; 238.89 mbsf) from 59 cm deeper in the core than sample BG831 has an apparent age of 270 kyr, a minimum age of 180 kyr and a maximum age of 370 kyr based on Sr isotopes [*Quinn et al.*, 1994]. A coral sample from 85.22 m deeper in the core than sample BG831 (831B-27R-CC, 12–14; 323.52 mbsf) has nearly concordant ages of 371 ± 9 kyr (^{230}Th) and 393 ± 11 kyr (^{234}U/^{238}U) and an initial δ^{234}U value of 159 ± 7. The age of sample BG831 can also be estimated using a stratigraphic forward model (see section 4.2). Tectonic subsidence rates can be calculated given the present elevation of a sample, the age of a sample, and the elevation of sea level at the time of coral growth [*Imbrie et al.*, 1984; *Shackleton*, 2000]). A minimum estimate of subsidence rate is 3.41 m/kyr ([1389.52 − 10.05]/[393 + 11]); an average estimate of subsidence rate is 3.50 m/kyr ([1389.52 − 47.95]/[[362 + 404]/2]); and a maximum estimate of subsidence rate is 3.66 m/kyr ([1389.52 − 65.42]/[371 − 9]). This range of subsidence rates is used as input to a stratigraphic forward model to calculate the age of coral sample BG831; minimum likely age, 335 ka; mean likely age, 341 ka; maximum likely age, 374 ka (Figure 3).

5.2. Assessment of Diagenetic Alteration

[30] Stratigraphic forward modeling can be used to demonstrate that coral sample BG831 was quickly submerged below the range of sea-level fluctuations shortly after deposition (Figure 3). Hence, sample BG831 has not likely ever been subaerially exposed nor has it been subjected to the ravages of freshwater diagenesis. Any postdepositional alteration of sample BG831 is likely restricted to those processes attendant with residence in marine waters and pore fluids.

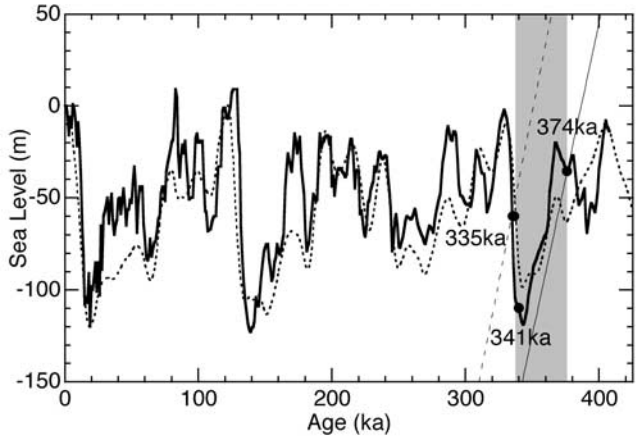

Figure 3. Stratigraphic forward modeling results. The age of sample BG831 is estimated on the basis of the zero-age depth of sample BG831, subsidence rate, and sea-level history. Sea level for the past 450 kyr is from the SPECMAP stack of global oxygen isotope variations (thick black line; *Imbrie et al.* [1984]) and from reconstructed $\delta^{18}O_{sw}$ variations (thin dotted line; *Shackleton* [2000]). Subsidence rates are estimated on the basis of convergence rate considerations [*Taylor et al.*, 1994]. Subsidence rates estimates range from a minimum rate of 3.4 m/kyr (coarsely dashed line) to a maximum rate of 3.7 m/kyr (thin, solid line). The intersections of the subsidence lines and the *Shackleton* [2000] sea-level curve place the age of coral sample BG831 between 335 and 374 ka (denoted by the vertical gray bar). The point representing 341 ka is the intercept of the central subsidence rate (3.5 m/kyr) calculated as explained in the text.

[31] Sample BG831 was examined for physical evidence of diagenetic alteration. X-ray diffraction analyses revealed only the presence of aragonite; no calcite peaks were identified, as expected from an originally aragonite sample that has never been subaerially exposed. Scanning electron microscopy (SEM) revealed no secondary cements (aragonite or calcite) in sample BG831. SEM images of a modern *Porites* coral sample are strikingly similar to those of the fossil coral sample BG831 (Figure 4). Examination of a petrographic thin section of sample BG831 documents similar preservation between modern and fossil coral; neither secondary cements nor recrystallization are discernable. A photomicrograph of the BG831 thin section is strikingly similar to a thin section photomicrograph of a well-preserved fossil coral from Papua New Guinea [*McGregor and Gagan*, 2003, Figure 3].

5.3. Geochemical Data

[32] The stable isotope ratios and Sr/Ca ratios used in this study were obtained for the entire 12 cm length of BG831 and the first 26 cm of MCB. The data from BG831 and MCB both show clear annual cycles in all of the measured geochemical variables. BG831 grew at an average rate of 9.8 mm/year and MCB grew at 20.0 mm/year. All significance tests and confidence intervals were calculated with same the number of degrees of freedom as years in the records. This assumes that there is one independent data point per year in these serially correlated records.

[33] Mean Sr/Ca ratios in the fossil and modern corals are significantly different with greater than 95% confidence (Figure 5). The mean Sr/Ca ratios for BG831 and MCB are 8.986 ± 0.018 mmol/mol and 8.881 ± 0.016 mmol/mol respectively (1σ). However, the mean annual cycles are very similar (Figure 6). The average annual Sr/Ca range is 0.13 ± 0.05 mmol/mol and 0.11 ± 0.04 mmol/mol (2σ) for BG831 and MCB, respectively. Calibration of the monthly-resolved modern coral Sr/Ca record 1980–1992 to GISST 2.3b SST over the same time period yields a slope of −0.050 ± 0.05 mmol/mol $°C^{-1}$ and a good correlation (r = −0.78).

[34] BG831 has a mean oxygen isotope ratio of −4.25 ± 0.07‰ VPDB (2σ, Vienna Peedee belemnite), whereas the mean MCB value is −4.99 ± 0.13‰ VPDB (2σ, Figure 5). They are different at the >99.9% confidence level. The annual $\delta^{18}O$ range averages 0.27 ± 0.10‰ in BG831, compared to a value of 0.45 ± 0.23‰ in MCB (Figure 6).

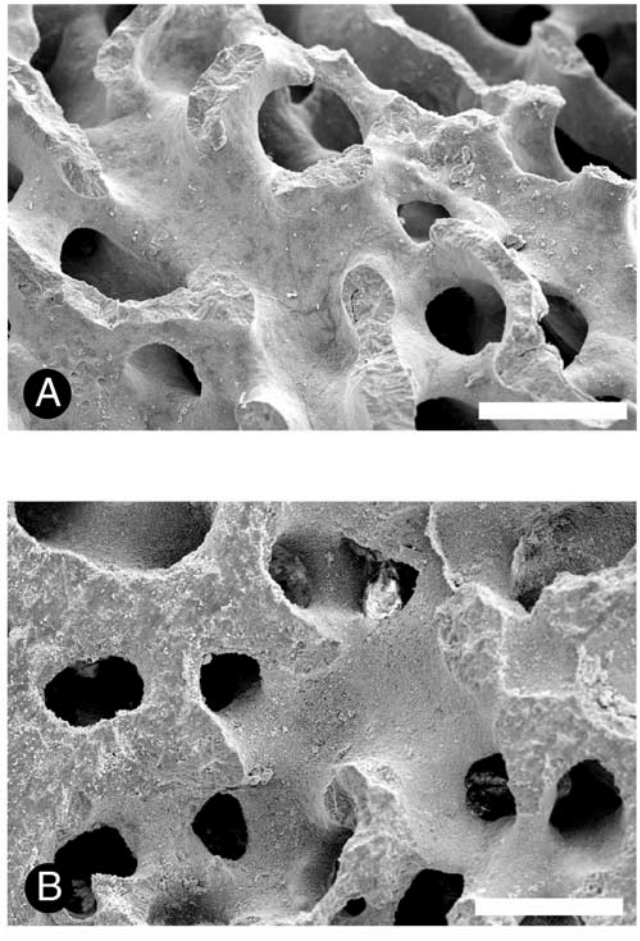

Figure 4. (a) Scanning electron microscope images of the modern coral MCB and (b) the fossil coral BG831. The scale bars are 50 μm in both images. The similarity of these images is evidence of the unaltered skeletal structure of the fossil coral.

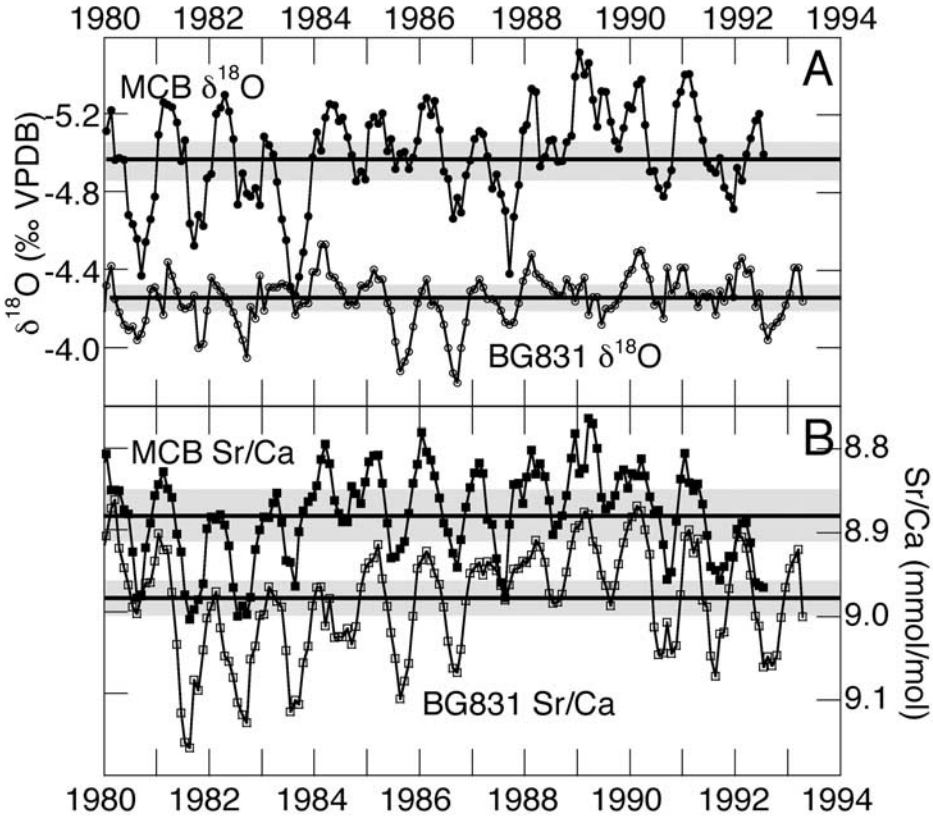

Figure 5. (a) Monthly $\delta^{18}O$ (b) and Sr/Ca time series for modern (MCB; filled circles) and fossil (BG831; open circles) corals. The mean value of each time series is denoted by solid horizontal lines; confidence levels (95% for $\delta^{18}O$ and Sr/Ca) are denoted by shaded rectangles. The fossil and modern corals have significantly different mean $\delta^{18}O$ and mean Sr/Ca values.

Part of the difference between the two $\delta^{18}O$ means must be due to the mean temperature difference indicated by the Sr/Ca data. Removing the Sr/Ca temperature signal from the oxygen isotope offset with the Sr/Ca-SST calibration above and the $\delta^{18}O$-SST calibration of *Gagan et al.* [1998] leaves 0.38‰ to be explained by a combination of salinity and ice volume. One cannot determine from this residual $\delta^{18}O$ value alone whether it results from a small positive change due to increased ice volume and a small positive change due to increased salinity, or a larger positive change due to increased ice volume and a negative change due to decreased salinity. A model is put forth in section 6.2 to examine these possibilities.

6. Discussion

6.1. Geochemical Evidence for Fossil Coral Preservation

[35] The Sr/Ca, oxygen isotope, and carbon isotope data provide good evidence that the coral has not undergone significant diagenesis. Precipitation of secondary calcite and recrystallization of coral aragonite to calcite causes a sharp decrease in Sr/Ca values (toward 0.4–2 mmol/mol from 8 to 9 mmol/mol; *Katz et al.* [1972]; *McGregor and Gagan* [2003]). The large difference in Sr/Ca between inorganic calcite and coral aragonite implies that a 1% contamination of coral aragonite by inorganic calcite would cause significant irregularities (up to 1.8°C) in the seasonal cycle [*Enmar et al.*, 2000; *McGregor and Gagan*, 2003]. Thus the retention of smooth annual cyclicity in Sr/Ca ratios in the fossil coral is consistent with preservation of a primary geochemical signal. Secondary aragonite has a slightly higher Sr/Ca ratio than coral aragonite [*Enmar et al.*, 2000; *Müller et al.*, 2001]. Contamination of a coral aragonite sample with 2% secondary aragonite, an amount unlikely to be missed by petrographic inspection, would cause a SST error of ~−0.5°C, about equal to the error in the calculations to derive temperature (see section 6.2). Calcitization of coral aragonite in the meteoric environment changes the original oxygen and carbon isotope values of the coral aragonite [e.g., *Pingitore*, 1976; *Martin et al.*, 1986] and disrupts the seasonal cycle as recorded by geochemical variation in the coral skeleton [e.g., *Hughen et al.*, 1999; *Tudhope et al.*, 2001]. Inorganic aragonite or high-magnesium calcite precipitation from marine waters would also increase the carbon isotope values by several per mil [*James and Choquette*, 1983; *McConnaughey*, 1989], but such an increase is not observed in the BG831 carbon isotope record. The balance of evidence

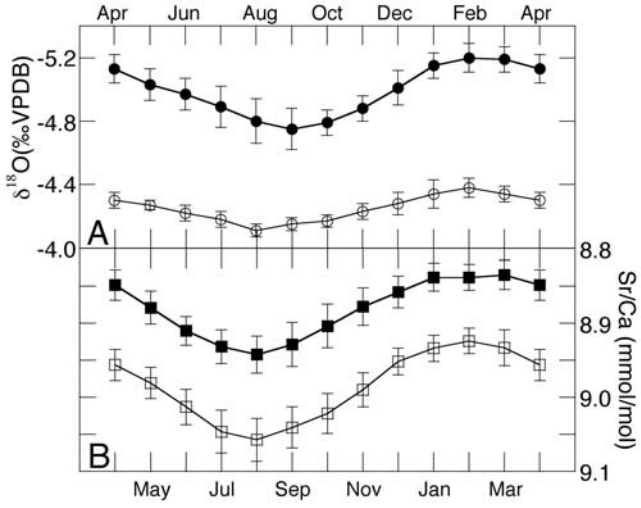

Figure 6. (a) Climatological mean annual cycle of coral $\delta^{18}O$ and (b) Sr/Ca in fossil coral BG831 (open symbols) and modern coral MCB (closed symbols). Error bars are 95% confidence intervals on the monthly means. The seasonal ranges of Sr/Ca in the MCB and BG831 are not significantly different from each other, implying that the seasonal temperature ranges at Vanuatu ~350 ka were similar to today. Conversely, the seasonal $\delta^{18}O$ range in the fossil coral is much smaller than the modern seasonal range, implying weaker seasonal hydrologic variations during the time of fossil coral growth.

causes us to reject the hypothesis that sample BG831 has been significantly altered by postdepositional processes.

6.2. Modeling the Pleistocene Mean Climate State

[36] Modern climate reconstructions essentially utilize the relationships between Sr/Ca, $\delta^{18}O$, salinity, and temperature to solve two equations for two unknowns. Sr/Ca is used to calculate temperature, which is then input into the $\delta^{18}O$ temperature equation, theoretically yielding $\delta^{18}O_{sw}$, a variable directly related to salinity. However, over geologic timescales these relationships may not be so straightforward.

[37] Unlike modern climate reconstructions, changes in seawater chemistry must be accounted for when interpreting Pleistocene coral records. Over glacial/interglacial timescales, the oxygen isotopic composition of seawater changes with ice volume due to the effects of preferential evaporation and sequestration of ^{16}O in glacial ice. This effect is well documented and the global average is 1.0 ± 0.1 ‰ for 120 m (sea-level equivalent) of ice build-up [e.g., *Schrag et al.*, 2002]. The Sr/Ca ratio of the ocean may also change as a function of ice volume because a low sea level exposes Sr-rich shelf carbonates to meteoric dissolution and recrystallization [*Stoll and Schrag*, 1998]. In contrast to $\delta^{18}O_{sw}$, seawater Sr/Ca variations over glacial/interglacial timescales are not well known. Model results of *Stoll and Schrag* [1998] indicate that seawater Sr/Ca may have increased by 1–3% during glacial periods, but the change in seawater Sr/Ca since the last glacial maximum was more likely 0.5–1.1% [*Stoll et al.*, 1999]. Some data agree with this model output, but more data are needed to verify the model predictions of the *Stoll and Schrag* [1998] and *Stoll et al.* [1999].

[38] A simple mathematical, mass balance model has been developed to investigate the effects of changing ocean chemistry on fossil coral Sr/Ca and $\delta^{18}O$. The following two equations were simultaneously solved under variable seawater Sr/Ca conditions and variable ice volume inputs:

$$\Delta Sr = \frac{\partial Sr}{\partial T} \times \Delta T + \frac{\partial Sr}{\partial I} \times \Delta I \quad (1)$$

$$\Delta O = \frac{\partial O}{\partial T} \times \Delta T + \frac{\partial O}{\partial I} \times \Delta I + \frac{\partial O}{\partial S} \times \Delta S, \quad (2)$$

where ΔSr is the difference between the modern Sr/Ca and fossil Sr/Ca ratios (fossil minus modern), and ΔO is similarly the difference between modern and fossil $\delta^{18}O$. The variables ΔT, ΔI, and ΔS are changes in temperature, ice volume, and salinity respectively, from modern to ancient times. The partial derivative terms are empirically determined and the values used are listed in Table 1.

[39] Two constraints on the equations are essential for limiting the domain and range of the equations. First, we know that the maximum change in ice volume over glacial/interglacial cycles is equivalent to about 120 m of sea level and that we are currently at a sea-level highstand (ice-volume low). Sea level can be further constrained from the age of the sample. Results of stratigraphic forward modeling suggest that BG831 grew while sea level was between 119 and 20 m below present sea level (Figure 3). Thus the ΔI term is constrained to between 20 and 119 m. Second, seawater Sr/Ca could not theoretically change more than 5% in any glacial/interglacial cycle and is more likely to be <3% [*Stoll et al.*, 1999]. The mathematical model was run several times, each time the ∂Sr/∂I term was held at different values.

[40] The full range of possible model results of SST and SSS are illustrated in Figure 7. Straight lines in Figure 7 denote different values for the ∂Sr/∂I term in the model, the boundaries of which are limited by maximal and minimal ice volumes. All of the lines converge on a single point that represents seawater $\Delta^{18}O$ and Sr/Ca values the same as today (i.e., no change in ice volume). Increasing the amount of Sr/Ca change on glacial-interglacial cycles causes an increase in the temperature uncertainty, whereas decreasing

Table 1. Definition of Variables Used to Solve Equations (1) and (2) for Sea-Surface Temperature, Ice Volume, and Sea Surface Salinity

Symbol	Values Used	Source
$\partial O/\partial T$[a]	−0.18‰/°C	*Gagan et al.* [1998]
$\partial O/\partial I$[b]	0.00833‰/m	*Schrag et al.* [2002]
$\partial O/\partial S$[c]	0.265‰/psu	*Fairbanks et al.* [1997]
$\partial Sr/\partial T$[d]	−0.050 mmol/mol °C^{-1}	this study
$\partial Sr/\partial I$[e]	0–3% per 120 m ice	*Stoll and Schrag* [1998]

[a]Change in coral $\delta^{18}O$ (‰ VPDB) per 1°C change in SST.
[b]Change in coral $\delta^{18}O$ (‰ VPDB) per 1 m change in sea level.
[c]Change in coral $\delta^{18}O$ (‰ VPDB) per 1 psu change in salinity.
[d]Change in coral Sr/Ca (mmol/mol) per 1°C change in SST.
[e]Change in coral Sr/Ca (mmol/mol) per 120 m change in sea level.

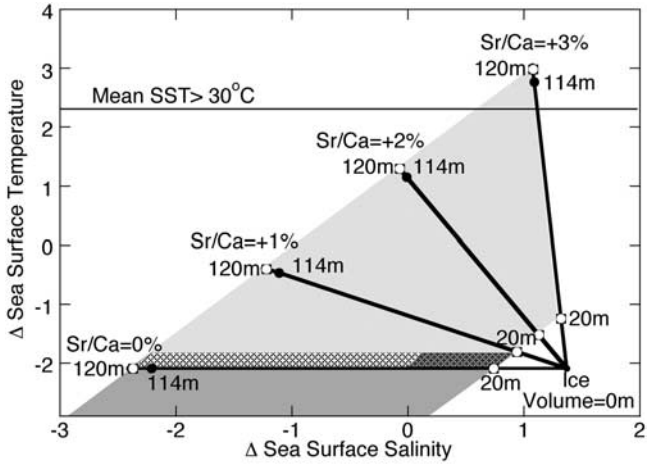

Figure 7. The model solution set of SST (ΔT, °C) and SSS (ΔS) changes at ~350 ka relative to the modern given a range of potential seawater Sr/Ca changes relative to modern. The plot is limited to those SST and SSS values that correspond to ice volume changes <120 m lower than present sea-level elevation. Squares with open circles represent the maximum and minimum ice-volume boundaries resulting from stratigraphic forward modeling (see Figure 3). Black circles denote the central date and ice volume obtained by forward stratigraphic modeling (see Figure 3). A thin black horizontal line denotes a mean annual SST of 30°C, a value assumed to be the upper bound of possible mean annual SST in this region. The light gray area illustrates the full range of solutions given the model input used. The medium gray shaded polygon represents average coral Mg/Ca-SST estimates, and the light and dark crosshatched regions represent the overlap between the Sr/Ca-δ^{18}O model and the Mg/Ca data solutions. The best estimate of actual conditions is shown in the light crosshatch pattern and represents surface conditions ~2°C cooler and 0–2 psu fresher than modern conditions at Santo.

the amount of Sr/Ca change on glacial-interglacial cycles causes an increase in the uncertainty of salinity.

[41] The model output (Figure 7) must be interpreted in light of other information to determine a mostly likely paleoclimate solution from the full range of model possibilities. A light gray parallelogram in Figure 7 represents temperature and salinity solutions limited by the age model and sea-level considerations. Thermodynamic processes may limit mean annual SST to no more than about 30°C [*Ramanathan and Collins*, 1991; *Cubukcu and Krishnamurti*, 2002]. This is mentioned because it may be useful with other data in other locations although it is not a useful constraint in this case, since the modern mean annual SST at Santo is 27.7°C and the maximum SST increase possible is close to the upper limits of the model.

[42] In this case, we use a less commonly used coral temperature proxy, Mg/Ca ratios, to constrain our model. Coral Mg/Ca can be used because seawater Mg/Ca is not thought to vary on glacial/interglacial timescales [e.g., *Hastings et al.*, 1998]. The difference between the modern and the fossil coral mean Mg/Ca indicates that temperatures were 2.4 ± 0.5 °C cooler when the fossil coral grew, using the in situ temperature calibration of *Quinn and Sampson* [2002]. A slightly darker shaded parallelogram represents the model results consistent with the Mg/Ca temperature and the error associated with the temperature calculations. The area of overlap between the Sr/Ca and δ^{18}O defined temperature and salinity, and the Mg/Ca defined temperature, denoted by the crosshatch pattern, represents the best estimate of surface ocean conditions ~350 ka. Data from fossil coral BG831 indicates that the surface ocean ~350 ka was ~2°C cooler. Salinity estimates are not as well constrained as SST estimates because of the age range of the fossil coral permits a wide range of sea-level possibilities (119 m to 20 m lower than the present). Our best estimate of SSS ~ 350 ka is that it was most likely 0–2 psu fresher than today. The 0–2 psu salinity change corresponds to an ice volume ≥43 m lower than the present; a condition that is met for ~73% of the age range of the fossil coral. Furthermore, the central age estimate of the fossil coral of 341 ka, the most probable true age of the coral, corresponds to an ice volume of −114 m with respect to modern.

[43] Lacking the additional SST constraints derived from coral Mg/Ca, the potential of changing seawater Sr/Ca on glacial/interglacial timescales contributes the most uncertainty in the SST and SSS determinations. As an example, if a paleo-sea-level elevation was known to be 120 m below present, then there would still be a SST and SSS uncertainty of 5.1°C and 3.7 psu, respectively, simply from not knowing if seawater Sr/Ca at 350 ka was the same as today or if it was greater than today's value by up to 3%. This demonstrates that accurate estimates of past seawater Sr/Ca values remain the largest obstacle to the accurate reconstruction of tropical SST in the past using Sr/Ca and δ^{18}O in pristine fossil corals.

[44] Mg/Ca determinations on fossil coral samples may provide a means by which to investigate the magnitude of glacial/interglacial changes in seawater Sr/Ca. Coral Mg/Ca-SST estimates from BG831 imply that seawater Sr/Ca ~350 ka was not considerably different from modern values. If true, this contrasts with previous seawater Sr/Ca estimates based on model results and foraminiferal data [e.g., *Stoll and Schrag*, 1998; *Stoll et al.*, 1999]. More work is clearly needed to better define the role that fossil coral Mg/Ca determinations might play in constraining glacial/interglacial changes in seawater Sr/Ca.

[45] Propagating the error in equations (1) and (2) [*Beers*, 1957, equation (37); *Schmidt*, 1999], demonstrates that the model SST and SSS values are robust. The exact magnitude of the standard error is dependent on the ice volume (ΔI) and temperature (ΔT) derived from the model, but is close to 0.5°C and 0.5 psu in all cases. The largest sources of error are the lengths of the coral geochemical records, specifically the variance in the mean value of each record. The second largest source of error is the ∂Sr/∂T relationship. Essentially, the more sensitive the paleothermometer, the greater the possible error associated with it.

[46] Equation (2) assumes that $\delta^{18}O_{sw}$ is only a function of global ice volume and local salinity (due to mixing with meteoric waters of unchanging isotopic compositions), but

there are other possibilities. One could change the relationship of $\delta^{18}O_{sw}$ and SSS by changing the isotopic composition of meteoric waters either by changing the source location for local precipitation or by changing the temperature of that source location [*Charles et al.*, 2001]. A model of the isotopic composition of precipitation during glacial times (forced with both CLIMAP SST and with cooler tropical SST fields) indicates that the $\delta^{18}O$ of precipitation around Santo would increase slightly during glacial times [*Charles et al.*, 2001]. Similarly, the $\delta^{18}O$ of precipitation in the eastern tropical Pacific would also generally increase, and that might increase the isotopic composition of the South Equatorial Current, which bathes Santo today [*Reverdin et al.*, 1994; *Qu and Lindstrom*, 2002]. The coral may record an isotopic enrichment due to a combination of increased isotopic composition of rainfall or increased isotopic value of the South Equatorial Current.

[47] How representative is a 13-year record of SST relative to multidecadal to century long SST records? Is it possible that the environmental changes evident in the fossil coral only represent a short-term shift rather than the mean state over a longer period? This issue is addressed in two ways. First, 13-year moving averages of monthly Sr/Ca and $\delta^{18}O$ data from the entire modern Santo coral (1928–1992; data not shown) documents that the mean for any 13-year period is never outside of the 95% confidence level on the mean Sr/Ca and $\delta^{18}O$ calculated from the full records (8.93 ± 0.03 mmol/mol and −4.85 ± 0.12 for Sr/Ca and $\delta^{18}O$ respectively). Second, 13-year moving averages of monthly SST data for the 20th century were used to demonstrate that this proxy-based conclusion is also robust when instrumental data are used. The mean SST value over the same time period was 27.57 ± 0.57°C and similarly to the results from the proxy record, the minimum and maximum 13-year mean were well within the error on the total mean value (27.27°C and 27.79°C for minimum and maximum respectively). Thus a 13-year record is representative of multidecadal to century long SST records and the mean value is not likely to be strongly affected by higher frequency oscillations.

6.3. Paleoclimatic Implications of Fossil Coral Data and Model Results

6.3.1. Paleoclimate of the Santo Region

[48] The seasonal range in $\delta^{18}O$ is smaller in the fossil record than in the modern record, whereas the seasonal range in Sr/Ca is the same in both fossil and modern corals (section 5.3). These differences in the seasonal cycles of $\delta^{18}O$ and Sr/Ca in the fossil and modern corals may be used to investigate the source of seasonal variability at Santo.

[49] Seasonal-scale salinity changes in the Santo region today are due to the migration of the SPCZ and the SSS front associated with it. The smaller amplitude annual cycle of $\delta^{18}O$ in BG831 relative to the modern must be due to seasonal hydrologic variations in ancient times because ice-volume effects are not possible on seasonal timescales, and the difference cannot be attributed to temperature because the seasonal Sr/Ca changes (i.e., SST changes) are similar in amplitude between modern and fossil records. There are two possible hydrologic scenarios that are consistent with the reduced amplitude $\delta^{18}O$ cycle in the fossil coral relative to the modern coral: a decrease in rain during the rainy season or an increase in rain during the dry season. The latter scenario is more consistent with our modeling results, which suggest a lower mean salinity ~350 ka with respect to today. One mechanism by which to increase rainfall during the austral winter is to limit the northward migration of the SPCZ during this season. This limited migration of the SPCZ at 350 ka contrasts with present-day austral winter migration of the SPCZ, which occurs in response to increasing Northern Hemisphere temperatures and convergence of the wind fields in a more northerly location. A more southerly position of the SPCZ at 350 ka is consistent with increased meridional thermal gradients in the Northern Hemisphere during glacial times [*Trent-Staid and Prell*, 2002].

[50] Reduced amplitude cycles in the fossil $\delta^{18}O$ are not likely the result from under-sampling of the slower-growing fossil coral because the sampling resolution was increased proportionally for the fossil coral. Furthermore, the continued success of studies showing primary Sr/Ca dependence on temperature [e.g., *Houck et al.*, 1977; *Smith et al.*, 1979; *Beck et al.*, 1992, 1997; *Eisenhauer et al.*, 1999; *Hughen et al.*, 1999; *Gagan et al.*, 2000; *Al-Rousan et al.*, 2002; *Marshall and McCulloch*, 2002; *Quinn and Sampson*, 2002] has diminished initial concerns over the growth-rate dependence of Sr/Ca in coral skeletons [*Weber*, 1973; *de Villiers et al.*, 1995].

[51] Could the fossil coral represent a single decadal-scale shift in the SPCZ as has occurred this century due to shifts in the Interdecadal Pacific Oscillation? The difference in $\delta^{18}O$ between the modern and the fossil is much larger than $\delta^{18}O$ variations recorded by the modern coral (1928–1992) which are thought to originate from modern shifts in rainfall linked to IPO movements. It is therefore unlikely that the fossil coral represents a similarly scaled event, but instead represents a larger spatial displacement of organized convection.

6.3.2. Paleoclimate of the Tropical Indo-Pacific

[52] The age estimate for fossil coral BG831 allows for the possibility that this coral grew when sea level was 20 to 119 m lower than today. The age estimate is centered close to the minimum sea level of MIS 10, so there is a higher likelihood that the coral grew during the glacial period than at the extreme edges of the age estimate, when sea levels were only 20 m lower than today. Additionally, 2–3°C of tropical cooling indicated by the coral geochemical data is more consistent with coral growth during a glacial period. We find it most reasonable therefore, to compare our results with studies of other glacial periods.

[53] The 2–3°C cooling at Santo, as indicated by the Mg/Ca ratios and supported by the Sr/Ca-$\delta^{18}O$ model, is consistent with other paleoclimate studies in the Pacific. Foraminiferal Mg/Ca ratios indicate ~3°C cooling in the western tropical Pacific during the last glacial maximum (LGM; MIS 2) and other glacial stages over the past 450 kyr (tropical South China Sea [*Stott et al.*, 2002]; Ontong Java Plateau [*Lea et al.*, 2000]; Sulu Sea [*Oppo et al.*, 2003]). Further evidence for cooling of this area during the LGM comes from modern analog technique-based faunal analysis at ODP site 828A, just west of Espiritu Santo Island,

which suggests at least 1–2°C cooling [*Barrows et al.*, 2000]. There has been much discussion of how much the tropics change during glacial periods (see *Trent-Staid and Prell* [2002] for a recent summary). Our data fall into the growing consensus that the tropical Pacific generally cooled by 2–3°C during glacial periods.

[54] Salinity decreases in the surface waters of the western equatorial Pacific (WEP) during glacial periods have been suggested by *Lea et al.* [2000] based on estimates of glacial seawater $\delta^{18}O$ that were lower than estimates of the global ocean value and those from the eastern equatorial Pacific (EEP). Our model results (Figure 7) are consistent with decreased surface salinity in the WEP during glacial periods. To have more than a slight salinity increase ~350 ka, one must assume that fossil coral BG831 grew during an interglacial period. While this is possible, stratigraphic modeling results and the depressed SST indicate that this scenario for coral growth is not likely.

[55] Planktonic foraminiferal $\delta^{18}O$ and Mg/Ca ratio data from the WPWP indicates a moderate salinity increase during the LGM along the eastern edge of the Indonesian archipelago [*Stott et al.*, 2002]. At first, the data from *Stott et al.* [2002] appear to directly conflict with the data from this study and that of *Lea et al.* [2000], which indicate decreasing salinity in the WEP during glacial periods. *Stott et al.* [2002] attempted to reconcile this conflict by pointing out that the Ontong Java Plateau (OJP) receives large increases in rainfall during ENSO warm phase events as the locus of atmospheric convection shifts eastward from Indonesia. If atmospheric convection also shifted eastward during glacial periods, seawater around Indonesia might become more saline, and seawater at other locations (such as the OJP) might become less saline. With this scenario, Santo would also experience increased salinity, as it does during an ENSO warm phase event, but the fossil coral data indicate conditions were actually less saline. A scenario that fits all of the data is that the northward, seasonal migrations of both the ITCZ and the SPCZ ~350 ka was more limited relative to today (i.e., both convergence zones remained closer to the austral summer configuration throughout the year). This would have the effect of shifting the mean salinity fields to the south, freshening Santo and the Ontong Java Plateau while leaving Indonesia saltier relative to modern conditions.

[56] Fully coupled atmosphere ocean general circulation models (AOGCMs) have recently been used to simulate LGM climate phenomena [*Bush and Philander*, 1998, 1999; *Hewitt et al.*, 2001; *Kitoh et al.*, 2001; *Kitoh and Murakami*, 2002; *Kim et al.*, 2003]. Seasonality in the convergence zones has not yet been studied, however some patterns can be identified. Tropical SSTs are lower in the models, as is average humidity. The hydrologic cycle is generally diminished, but each model seems to have some regions where tropical convergence increases along with the P-E balance. The model used by *Kim et al.* [2003] displays stronger trade winds and an increase in Walker circulation coincident with a decrease in ITCZ activity. The SPCZ (the upward limb of Walker circulation) is shifted slightly westward and SSS decreases compared to modern day beneath the convergence zone. This scenario can explain decreased average SSS at Santo and increases in SSS in Indonesia, an area usually doused with rainwater from the ITCZ, although it does not explain the freshening of the Ontong Java Plateau at the LGM.

[57] Model evidence for increased trade winds is further supported by other paleo data. Factor analysis of planktonic foraminifera data indicate an increased thermocline tilt, and thus stronger trade wind activity during the LGM [*Andreasen and Ravelo*, 1997]. SST data from foraminiferal assemblage work similar to the CLIMAP project [*CLIMAP Project Members*, 1976, 1981] suggest an increased zonal thermal gradient across the Pacific Ocean, further supporting an increase in the trade winds [*Trend-Staid and Prell*, 2002]. Admittedly, the coupled models result in SSTs that are cooler than the foraminiferal data indicate, but otherwise the general patterns are similar.

[58] In summary, reconstructing the hydrologic response to glacial forcing is a complex issue. Much evidence exists for stronger trade winds that would tilt the tropical thermocline to the west and encourage stronger Walker circulation that could in turn decrease salinity in surface waters beneath the SPCZ. Additional "paleo" data are needed to constrain the east-west thermal and salinity gradients across the Pacific Ocean during glacial periods, and to help resolve the discrepancies in current model and climate proxy results.

6.4. Modern and Pleistocene Interannual Variability

[59] The response of coral $\delta^{18}O$ and Sr/Ca to interannual SST and SSS forcing must be demonstrated in the modern records before interannual relationships in the fossil record can be considered. ENSO warm (cold) phase events are manifest in this region as cool (warm) and dry (wet) anomalies [*Delcroix*, 1998]. Corals respond to lower (higher) SST and higher (lower) SSS values attendant with an ENSO warm (cool) phase by precipitating skeletal material that has higher (lower) $\delta^{18}O$ and Sr/Ca values.

[60] The $\delta^{18}O$ and Sr/Ca anomaly plots from MCB are very similar to the SSSA and SSTA plots from Santo (Figure 2). Coral $\delta^{18}O$ and Sr/Ca both increase during the 1983, 1987, and 1991 El Niño events, and they decrease in the 1989 La Niña event. Additionally, modern coral geochemistry provides details about the characteristics of each event that we know to be true from the instrumental record. The 1983 warm phase event was characterized in the region by a large salinity anomaly and a small temperature anomaly. Salinity in the western Pacific lagged behind the eastern Pacific warming (represented by gray bars in Figure 2) during this event. The timing and relative magnitude of temperature and salinity anomalies in the proxy data match the instrumental records well (Figure 2). The 1987 ENSO event was manifest in this region by large temperature anomalies and smaller salinity anomalies; a scenario well recorded by the proxy data (Figure 2). By using the definition of ENSO events described in section 3, one can easily identify modern ENSO events in the geochemical proxy records, and even further describe details about the temperature and salinity anomalies associated with these events.

[61] The Sr/Ca and $\delta^{18}O$ time series in the fossil coral from Santo contain two geochemical excursions that are consistent with our definition of ENSO events as recorded in the geochemistry of a modern coral (see section 3; Figure 2). The first "paleo-ENSO" event is primarily manifest as a temperature anomaly that lasts for essentially 16 months. The positive Sr/Ca anomaly reaches the 1.5-σ threshold criterion in June of year 2, and continues through September of year 3, with a 4-month period in between where the anomaly remains positive, but drops below the threshold criterion of 1.5 σ. Meanwhile, the $\delta^{18}O$ anomaly does not increase until September of year 2, but remains primarily positive through September of year 3. The maximum SSTA is −1.8°C.

[62] The second "paleo-ENSO" event lasts 17 months and strictly speaking should be split into two events by our definition. Both proxies have anomalies during year 6 and again in year 7. The event is primarily recorded by a $\delta^{18}O$ anomaly, indicating that salinity deviations dominated this event. $\delta^{18}O$ reaches the 1.5 σ threshold criterion in July of year 6, drops below the threshold criterion in December of the same year, and then bounces back again in June through November of the following year. The Sr/Ca anomalies are minimal over this time, but they do show minor positive anomalies associated with the larger $\delta^{18}O$ positive anomalies.

[63] These two climate events, interpreted as "paleo-ENSO" events, appear to agree with the findings of *Tudhope et al.* [2001], who reported decreased interannual variability in coral $\delta^{18}O$ during glacial periods at Papua New Guinea. The absolute amplitudes of the $\delta^{18}O$ and Sr/Ca anomalies in BG831 are smaller than $\delta^{18}O$ and Sr/Ca anomalies observed in the modern coral. However, as a percentage of the average seasonal range, the anomalies are very similar to modern events. BG831 is too short of a record to divulge significant information about the frequency of "paleo-ENSO" events.

[64] ENSO variability may be controlled by the ~20 kyr precessional cycle [*Clement et al.*, 1999, 2000]. Seasonal variations in insolation are especially important in modulating ENSO in the geologic past [*Clement et al.*, 1999; *Kukla et al.*, 2002] and one would expect lower frequency of El Niño events at times when perihelion occurs in March and aphelion occurs in September of minimal seasonality in equatorial insolation (March minus September insolation is at a minimum). Such minima in the equatorial seasonality of equatorial insolation occurred at ~350 ka and during the last glacial period around 30 and 55 ka [*Laskar*, 1990].

7. Conclusions

[65] We have compared geochemical variations in a fossil coral with those from a modern coral from Espiritu Santo, Vanuatu to address two fundamental questions:

[66] 1. What was the background climate state of the tropical Pacific, in terms of temperature and salinity, during ~350 ka?

[67] 2. Is there evidence of ENSO activity at ~350 ka? This study confirmed that modern *Porites* spp. corals from Santo record significant surface-ocean variability in the $\delta^{18}O$ and Sr/Ca of their skeletons. Hydrologic and thermal details of specific ENSO events are in fact resolvable in the modern coral geochemical record.

[68] This study also confirmed that climatologically significant information can be preserved in the skeletal aragonite of fossil corals over long (10^5 years) timescales. Changes in seawater chemistry can have large affects on the climatological interpretation of fossil coral records and must be accounted for even if the geochemical signature of environmental variability is preserved in the fossil coral skeletons. A simple mathematical model using empirically derived relationships joining $\delta^{18}O$ and Sr/Ca with seawater Sr/Ca variations, seawater $\delta^{18}O$ variations, SST, and SSS, facilitates the interpretation of coral geochemical records.

[69] Specific conclusions include:

[70] 1. Coral proxy data and mathematical modeling of Pleistocene mean SST and SSS results in temperature estimates ~2°C cooler and salinity 0–2 psu fresher than present-day conditions. Our fossil coral data and modeling results preclude warmer SST and substantially higher SSS at Santo at ~350 ka. Accurate estimates of past values of seawater Sr/Ca remain the largest obstacle to the accurate reconstruction of tropical SST in the past using Sr/Ca from pristine fossil corals.

[71] 2. Seasonal SST ranges reconstructed ~350 ka are very similar to modern seasonal SST ranges. In contrast, seasonal hydrologic variations ~350 ka are reduced in amplitude relative to the modern. The reduced seasonal SSS variations and increased SSTs near Santo are interpreted as evidence that the SPCZ at ~350 ka did not migrate as far northward during austral winter as it does today.

[72] 3. ENSO or ENSO-like interannual variations are not unique to interglacial time periods, nor just the past 130 kyr, but are also present in the tropical southwestern Pacific between 335 and 374 ka.

[73] **Acknowledgments.** The authors thank Anthony Greco for assistance with SEM analyses, Thierry Corrège for his help with the initial method development for the ICP, and Ethan Goddard for all of his tireless efforts in the analytical laboratories at USF. The manuscript was enhanced through interactions with Benjamin Flower, David Hollander, and Gary Mitchum and through the comments of two anonymous reviewers.

References

Al-Rousan, S., S. Al-Moghrabi, J. Pätzold, and G. Wefer (2002), Environmental and biological effects on the stable oxygen isotope records of corals in the northern Gulf of Aqaba, Red Sea, *Mar. Ecol. Progr. Ser.*, *239*, 301–310.

An, S.-I., and B. Wang (2000), Interdecadal change of the structure of the ENSO mode and its impact on the ENSO frequency, *J. Clim.*, *13*, 2044–2055.

Andreasen, D., and A. C. Ravelo (1997), Tropical Pacific Ocean thermocline depth reconstructions for the Last Glacial Maximum, *Paleoceanography*, *12*, 395–414.

Bar-Matthews, M., G. J. Wasserburg, and J. H. Chen (1993), Diagenesis of fossil coral skeletons: Correlation between trace elements, textures, and $^{234}U/^{238}U$, *Geochim. Cosmochim. Acta*, *57*, 257–276.

Barrows, T. T., S. Juggins, P. de Deckker, J. Thiede, and J. I. Martinez (2000), Sea-surface temperatures of the southwest Pacific Ocean during the Last Glacial Maximum, *Paleoceanography*, *15*(1), 95–109.

Battisti, D. S., and A. C. Hirst (1989), Interannual variability in the tropical atmosphere-ocean system: Influence of the basic state and ocean geometry, *J. Atmos. Sci.*, *46*, 1687–1712.

Beck, J. W., R. L. Edwards, E. Ito, F. W. Taylor, J. Recy, F. Rougerie, P. Joannot, and C. Henin (1992), Sea-surface temperature for coral skeletal strontium/calcium ratios, *Science*, *257*, 644–647.

Beck, J. W., J. Recy, F. Taylor, R. L. Edwards, and G. Cabioch (1997), Abrupt changes in early Holocene tropical sea surface temperature derived from coral records, *Nature*, *385*, 705–707.

Beers, Y. (1957), *Introduction to the Theory of Error*, 66 pp., Addison-Wesley-Longman, Reading, Mass.

Bigg, G. R., and E. J. Rohling (2000), An oxygen isotope data set for marine waters, *J. Geophys. Res.*, *105*(C4), 8527–8535.

Bush, A. B. G., and S. G. H. Philander (1998), The role of ocean-atmosphere interactions in tropical cooling during the Last Glacial Maximum, *Science*, *279*, 1341–1344.

Bush, A. B. G., and S. G. H. Philander (1999), The climate of the Last Glacial Maximum: Results from a coupled atmosphere-ocean general circulation model, *J. Geophys. Res.*, *104*, 24,509–24,525.

Charles, C. D., H. Rind, and R. Webb (2001), Tropical cooling and the isotopic composition of precipitation in general circulation model simulations of the ice age climate, *Clim. Dyn.*, *17*, 489–502.

Clement, A. C., R. Seager, and M. A. Cane (1999), Orbital controls on the El Niño/Southern Oscillation and the tropical climate, *Paleoceanography*, *14*, 441–456.

Clement, A. C., R. Seager, and M. A. Cane (2000), Suppression of El Niño during the mid-Holocene by changes in the Earth's orbit, *Paleoceanography*, *15*, 731–737.

CLIMAP Project Members (1976), The surface of the ice-age Earth, *Science*, *191*, 1131–1137.

CLIMAP Project Members (1981), Seasonal reconstructions of the Earth's surface at the Last Glacial Maximum, *Geol. Soc. of Am. Map Chart Serv., MC36*, 1–18.

Craig, H., and L. I. Gordon (1965), Isotopic oceanography: Deuterium and oxygen 18 variations in the ocean and the marine atmosphere, in *Marine Geochemistry*, edited by D. R. Schink and J. T. Corless, pp. 227–374, Univ. of Rhode Island, Kingston, R. I.

Cubukcu, N., and T. N. Krishnamurti (2002), Low-frequency controls on the thresholds of sea surface temperature of the western tropical Pacific, *J. Clim.*, *15*, 1626–1642.

Delcroix, T. (1998), Observed surface oceanic and atmospheric variability in the tropical Pacific at seasonal and ENSO timescales: A tentative overview, *J. Geophys. Res.*, *103*(C9), 18,611–18,633.

de Villiers, S., B. K. Nelson, and A. R. Chivas (1995), Biological controls on coral Sr/Ca and $\delta^{18}O$ reconstructions of sea surface temperatures, *Science*, *269*, 1247–1249.

Dunbar, R. B., , and J. E. Cole (Eds.) (1999), Annual Records for Tropical Systems (ARTS), recommendations for research, *PAGES Workshop Rep., Ser. 99-1*, 72 pp., World Data Cent. A for Paleoclimatol., Boulder, Colo.

Edwards, R. L., J. H. Chen, and G. J. Wasserburg (1986), ^{238}U-^{234}U-^{230}Th-^{232}Th systematics and the precise measurement of time over the past 500,000 years, *Earth Planet. Sci. Lett.*, *81*, 175–192.

Edwards, R. L., C. D. Gallup, F. W. Taylor, T. M. Quinn, and ODP Leg 134 Scientific Party (1991), $^{230}Th/^{238}U$ and $^{234}U/^{238}U$ in submarine corals: Evidence for diagenetic leaching of ^{234}U, *Eos Trans. AGU*, *72*, 535.

Eisenhauer, A., D. Wischow, K. Wyrwoll, L. Collins, Z. Zhu, G. Heiss, C. Dullo, and B. Hansen (1999), Sr/Ca and U/Ca-thermometry of modern and fossil corals form the Abrolhos Islands and the Ningaloo Reef, Western Australia, *Eos Trans. AGU*, *80*(46), Fall Meet. Suppl., Abstract OS52A-18.

Enfield, D. B., and L. Cid (1991), Low-frequency changes in El Niño-Southern Oscillation, *J. Clim.*, *4*, 1137–1146.

Enmar, R., M. Stein, M. Bar-Matthews, E. Sass, A. Katz, and B. Lazar (2000), Diagenesis in live corals from the Gulf of Aqaba, I. The effect on paleo-oceanography tracers, *Geochim. Cosmochim. Acta*, *64*, 3123–3132.

Epstein, S., R. Buchsbaum, H. Lowenstam, and H. C. Urey (1953), Revised carbonate-water isotopic temperature scales, *Geol. Soc. Am. Bull.*, *64*, 1315–1326.

Fairbanks, R. G., M. N. Evans, J. L. Rubenstone, R. A. Mortlock, K. Broad, M. D. Moore, and C. D. Charles (1997), Evaluating climate indices and their geochemical proxies measured in corals, *Coral Reefs*, (16), suppl., S93–S100.

Fedorov, A. V., and S. G. Philander (2000), Is El Niño changing?, *Science*, *288*, 1997–2002.

Folland, C. K., J. A. Renwick, M. J. Salinger, and A. B. Mullan (2002), Relative influences of the Interdecadal Pacific Oscillation and ENSO on the South Pacific Convergence Zone, *Geophys. Res. Lett.*, *29*(13), 1643, doi:10.1029/2001GL014201.

Gagan, M. K., L. K. Ayliffe, D. Hopley, J. A. Cali, G. E. Mortimer, J. Chappell, M. T. McCulloch, and M. J. Head (1998), Temperature and surface-ocean water balance of the mid-Holocene tropical western Pacific, *Science*, *279*, 1014–1018.

Gagan, M. K., L. K. Ayliffe, J. W. Beck, J. E. Cole, E. R. M. Druffel, R. B. Dunbar, and D. P. Schrag (2000), New views of tropical paleoclimates from corals, *Quat. Sci. Rev.*, *19*, 45–64.

Goreau, T. J. (1977), Coral skeletal chemistry: Physiological and environmental regulation of stable isotopes and trace metals in *Montastraea annularis*, *Proc. R. Soc. London B*, *196*, 291–315.

Gouriou, Y., and T. Delcroix (2002), Seasonal and ENSO variations of sea surface salinity and temperature in the South Pacific Convergence Zone during 1976–2000, *J. Geophys. Res.*, *107*(C12), 8011, doi:10.1029/2001JC000830.

Hastings, D. W., A. D. Russell, and S. R. Emerson (1998), Foraminiferal magnesium in *Globeriginoides sacculifer* as a paleotemperature proxy, *Paleoceanography*, *13*(2), 161–169.

Henderson, G. M., A. S. Cohen, and R. K. O'Nions (1993), $^{234}U/^{238}U$ ratios and ^{230}Th ages for Hateruma Atoll corals: Implications for coral diagenesis and seawater $^{34}U/^{238}U$ ratios, *Earth Planet. Sci. Lett.*, *115*, 65–73.

Hewitt, C. D., A. J. Broccoli, J. F. B. Mitchell, and R. J. Stouffer (2001), A coupled model study of the Last Glacial Maximum: Was part of the North Atlantic relatively warm?, *Geophys. Res. Lett.*, *28*(8), 1571–1574.

Houck, J. E., S. V. Smith, and P. L. Jokiel (1977), The response of coral growth rate and strontium content to light intensity and water temperature, paper presented at Proceedings of the 3rd International Coral Reef Symposium, Rosenstiel Sch. of Mar. and Atmos. Sci., Univ. of Miami, Miami, Fla.

Hughen, K. A., D. P. Schrag, S. B. Jacobsen, and W. Hantoro (1999), El Niño during the last interglacial period recorded by a fossil coral from Indonesia, *Geophys. Res. Lett.*, *26*(20), 3129–3132.

Imbrie, J., J. D. Hays, D. G. Martinson, A. McIntyre, A. Mix, J. J. Morley, N. G. Pisias, W. Prell, and N. J. Shackleton (1984), The orbital theory of Pleistocene climate: Support from a revised chronology of the marine $\delta^{18}O$ record, in *Milankovitch and Climate*, edited by A. Berger et al., pp. 269–305, D. Reidel, Norwell, Mass.

James, N. P., and W. Choquette (1983), Diagenesis 6. Limestones—The sea floor diagenetic environment, *Geosci. Can.*, *10*, 162–179.

Katz, A., E. Sass, A. Starinsky, and H. D. Holland (1972), Strontium behavior in the aragonite-calcite transformation: An experimental study at 40°–90°C, *Geochim. Cosmochim. Acta*, *36*, 481–496.

Kim, S.-J., G. M. Flato, and G. J. Boer (2003), A coupled climate model simulation of the Last Glacial Maximum, part 2: Approach to equilibrium, *Clim. Dyn.*, *20*, 635–661, doi:10.1007/s00382-002-0292-2.

Kitoh, A., and S. Murakami (2002), Tropical Pacific climate at the mid-Holocene and the Last Glacial Maximum simulated by a coupled ocean-atmosphere general circulation model, *Paleoceanography*, *17*(3), 1047, doi:10.1029/2001PA000724.

Kitoh, A., S. Murakami, and H. Koide (2001), A simulation of the Last Glacial Maximum with a coupled atmosphere-ocean GCM, *Geophys. Res. Lett.*, *28*(11), 2221–2224.

Kukla, G. J., A. C. Clement, M. A. Cane, and J. E. Gavin (2002), Last interglacial and early glacial ENSO, *Quat. Res.*, *58*, 27–31.

Lagerloef, G., and T. Delcroix (1999), Sea surface salinity observations for the Tropical Pacific, *CLIVAR Exchanges*, *4*(3), 5–10.

Laskar, J. (1990), The chaotic motion of the solar system: A numerical estimate of the chaotic zones, *Icarus*, *88*, 266–291.

Lea, D. W., D. K. Pak, and H. J. Spero (2000), Climate impact of Late Quaternary equatorial Pacific sea surface temperature variations, *Science*, *289*, 1719–1724.

Levitus, S., and T. P. Boyer (1994), *World Ocean Atlas 1994*, vol. 4, *Temperature, NOAA Atlas NESDIS 4*, 117 pp., NOAA, Silver Spring, Md.

Marshall, J. F., and M. T. McCulloch (2002), An assessment of the Sr/Ca ratio in shallow water hermatypic corals as a proxy for sea surface temperature, *Geochim. Cosmochim. Acta*, *66*(18), 3263–3280.

Martin, G. D., B. H. Wilkinson, and K. C. Lohmann (1986), The role of skeletal porosity in aragonite neomorphism: Strombus and Montastrea from the Pleistocene Key Largo Limestone, Florida, *J. Sediment. Petrol.*, *56*, 194–203.

McConnaughey, T. (1989), ^{13}C and ^{18}O isotopic disequilibrium in biologic carbonates: I. Patterns, *Geochim. Cosmochim. Acta*, *53*, 151–162.

McCulloch, M. T., G. Mortimer, T. Esat, L. Xianhua, B. Pillans, and J. Chappell (1996), High resolution windows into early Holocene climate: Sr/Ca coral records from the Huon Peninsula, *Earth Planet. Sci. Lett.*, *138*, 169–178.

McCulloch, M. T., A. W. Tudhope, T. Esat, G. E. Mortimer, J. Chappell, B. Pillans, A. R. Chivas, and A. Omura (1999), Coral record

of equatorial sea-surface temperatures during the penultimate deglaciation at Huon Peninsula, *Science*, *283*, 202–283.

McGregor, H. V., and M. K. Gagan (2003), Diagenesis and geochemistry of Porites corals from Papua New Guinea: Implications for paleoclimate reconstruction, *Geochim. Cosmochim. Acta.*, *67*(12), 2147–2156.

Minobe, S. (1997), A 50–70 year climatic oscillation over the North Pacific and North America, *Geophys. Res. Lett.*, *24*, 6833–6836.

Minobe, S. (1999), Resonance in bidecadal and pentadecadal climate oscillations over the North Pacific: Role in climatic regime shifts, *Geophys. Res. Lett.*, *26*, 855–858.

Müller, A., M. K. Gagan, and M. T. McCulloch (2001), Early marine diagenesis in corals and geochemical consequences for paleoceanographic reconstructions, *Geophys. Res. Lett.*, *28*(23), 4471–4474.

Nitta, T., and S. Yamada (1989), Recent warming of tropical sea surface temperature and its relationship to the Northern Hemisphere circulation, *J. Meteorol. Soc. Jpn.*, *67*, 187–193.

Oppo, D. W., B. K. Linsley, Y. Rosenthal, S. Dannenmann, and L. Beaufort (2003), Orbital and suborbital climate variability in the Sulu Sea, western tropical Pacific, *Geochem. Geophys. Geosyst.*, *4*(1), 1003, doi:10.1029/2001GC000260.

Paillard, D., L. Labeyrie, and P. Yiou (1996), Macintosh program performs time-series analysis, *Eos Trans. AGU*, *77*, 379.

Parker, D. E., C. K. Folland, and M. Jackson (1995), Marine surface temperature: Observed variations and data requirements, *Clim. Change*, *31*, 559–600.

Picaut, J., M. Ioualalen, C. Menkes, T. Delcroix, and M. J. McPhaden (1996), Mechanism of the zonal displacements of the Pacific warm pool: Implications for ENSO, *Science*, *274*, 1486–1489.

Picaut, J., F. Masia, and Y. du Penhoat (1997), An advective-reflective conceptual model for the oscillatory nature of ENSO, *Science*, *277*, 663–666.

Picaut, J., M. Ioualalen, T. Delcroix, F. Masia, R. Murtugudde, and J. Vialard (2001), The oceanic zone of convergence on the eastern edge of the Pacific warm pool: A synthesis of results and implications for El Niño-Southern Oscillation and biogeochemical phenomena, *J. Geophys. Res.*, *106*(C2), 2263–2386.

Pingitore, N. E. (1976), Vadose and phreatic diagenesis: Processes, products and their recognition in corals, *J. Sediment. Petrol.*, *46*(4), 985–1006.

Qu, T. D., and E. J. Lindstrom (2002), A climatological interpretation of the circulation in the western South Pacific, *J. Phys. Oceanogr.*, *32*(9), 2492–2508.

Quinn, W. H., and T. Neal (1984), Recent climate change and the 1982–83 El Niño, paper presented at 8th Annual Climate Diagnostic Workshop, NOAA, Downsville, Ont., Canada.

Quinn, W. H., and T. Neal (1985), Recent long-term climate change over the eastern tropical and subtropical Pacific and its ramifications, paper presented at 9th Annual Climate Diagnostic Workshop, NOAA, Corvallis, Oreg.

Quinn, T. M., and D. E. Sampson (2002), A multiproxy approach to reconstructing sea surface conditions using coral skeleton geochemistry, *Paleoceanography*, *17*(4), 1062–1073.

Quinn, T. M., F. W. Taylor, and A. N. Halliday (1994), Strontium-isotopic dating of neritic carbonates at Bougainville Guyot (site 831), New Hebrides Island Arc, *Proc. Ocean Drill. Program Sci. Results*, *134*, 89–95.

Ramanathan, V., and W. Collins (1991), Thermodynamic regulation of ocean warming by cirrus clouds deduced from observations of the 1987 El Niño, *Nature*, *351*, 27–32.

Ren, L., B. K. Linsley, G. M. Wellington, D. P. Schrag, and O. Hoegh-Guldberg (2003), Deconvolving the $\delta^{18}O$ seawater component from subseasonal coral $\delta^{18}O$ and Sr/Ca at Rarotonga in the southwestern subtropical Pacific for the period 1726–1997, *Geochim. Cosmochim. Acta*, *67*(9), 1609–1621.

Reverdin, G., C. Frankignoul, E. Kestenare, and M. J. McPhaden (1994), Seasonal variability in the surface currents of the equatorial Pacific, *J. Geophys. Res.*, *99*, 20,323–20,344.

Rittenour, T. M., Brigham-GretteFnmJ., and M. E. Mann (2000), El Niño-like climate teleconnections in New England during the Late Pleistocene, *Science*, *288*, 1039–1042.

Rodbell, D. T., G. O. Seltzer, D. M. Anderson, M. B. Abbott, D. B. Enfield, and J. H. Newman (1999), An ~15,000-year record of El Niño-driven alluviation in southwestern Ecuador, *Science*, *283*, 516–520.

Sandweiss, D., J. Richardson, E. Reitz, H. Rollins, and K. Maasch (1996), Geoarchaeological evidence from Peru for a 5000 year onset of El Niño, *Science*, *274*, 1531–1533.

Schmidt, G. A. (1999), Error analysis of paleosalinity calculations, *Paleoceanography*, *14*(3), 422–429.

Schrag, D. P. (1999), Rapid analysis of high-precision Sr/Ca ratios in corals and other marine carbonates, *Paleoceanography*, *14*(2), 97–102.

Schrag, D. P., J. F. Adkins, K. McIntyre, J. L. Alexander, D. A. Hodell, C. D. Charles, and J. F. McManus (2002), The oxygen isotopic composition of seawater during the Last Glacial Maximum, *Quat. Sci. Rev.*, *21*, 331–342.

Shackleton, N. J. (2000), The 100,000-year ice-age cycle identified and found to lag temperature, carbon dioxide and orbital eccentricity, *Science*, *289*, 1897–1902.

Smith, S. V., R. W. Buddemeier, R. C. Redalje, and J. E. Houck (1979), Strontium-calcium thermometry in coral skeletons, *Science*, *204*, 404–407.

Stephens, C., S. Levitus, J. Antonov, and T. P. Boyer (2001), On the Pacific Ocean regime shift, *Geophys. Res. Lett.*, *28*(19), 3721–3724.

Stoll, H. M., and D. P. Schrag (1998), Effects of Quaternary sea-level cycles on strontium in seawater, *Geochim. Cosmochim. Acta.*, *62*(7), 1107–1118.

Stoll, H. M., D. P. Schrag, and S. C. Clemens (1999), Are seawater Sr/Ca variations preserved in Quaternary foraminifera?, *Geochim. Cosmochim. Acta*, *63*(21), 3535–3547.

Stott, L., C. Poulsen, S. Lund, and R. Thunell (2002), Super ENSO and global climate oscillation at millennial time scales, *Science*, *297*, 222–230.

Suarez, M. J., and P. S. Schopf (1988), A delayed action oscillator for ENSO, *J. Atmos. Sci.*, *45*, 3283–3287.

Taylor, F. W., T. M. Quinn, C. D. Gallup, and R. L. Edwards (1994), Quaternary Plate convergence rates at the New Hebrides island arc from the chronostratigraphy of Bougainville Guyot (site 831), *Proc. Ocean Drill. Program Sci. Results*, *134*, 47–57.

Trenberth, K. E. (1997), The definition of El Niño, *Bull. Am. Meteorol. Soc.*, *78*(12), 2771–2777.

Trenberth, K. E., and T. J. Hoar (1996), The 1990–1995 El Niño-Southern Oscillation event: Longest on record, *Geophys. Res. Lett.*, *23*, 57–60.

Trenberth, K. E., and T. J. Hoar (1997), El Niño and climate change, *Geophys. Res. Lett.*, *24*(23), 3057–3060.

Trenberth, K. E., and J. W. Hurrel (1994), Decadal atmosphere-ocean variations in the Pacific, *Clim. Dyn.*, *9*, 303–319.

Trent-Staid, M., and W. L. Prell (2002), Sea surface temperature at the Last Glacial Maximum: A reconstruction using the modern analog technique, *Paleoceanography*, *17*(4), 1065–1082.

Tudhope, A. W., C. P. Chilcott, M. T. McCulloch, E. R. Cook, J. Chappell, R. M. Ellam, D. W. Lea, J. M. Lough, and G. B. Shimmield (2001), Variability in the El Niño-Southern Oscillation though a glacial-interglacial cycle, *Science*, *291*, 1511–1517.

Vialard, J., and P. Delecluse (1998), An OGCM study for the TOGA decade. part I: Role of salinity in the physics of the western Pacific fresh pool, *J. Phys. Oceanogr.*, *28*, 1071–1088.

Vincent, D. G. (1994), The South Pacific Convergence Zone (SPCZ): A review, *Mon. Weather Rev.*, *122*, 1949–1970.

Wang, B., and S.-I. An (2001), Why the properties of El Niño changed during the late 1970s, *Geophys. Res. Lett*, *28*(19), 3709–3712.

Weber, J. N. (1973), Incorporation of strontium into reef coral skeletal carbonate, *Geochim. Cosmochim. Acta*, *37*(9), 2173–2190.

Weber, J. N., and P. M. J. Woodhead (1972), Temperature dependence of oxygen-18 concentration in reef coral carbonates, *J. Geophys. Res.*, *77*, 463–473.

Zebiak, S. E., and M. A. Cane (1987), A model El Niño-Southern Oscillation, *Mon. Weather Rev.*, *115*, 2262–2278.

K. H. Kilbourne and T. M. Quinn, College of Marine Sciences, University of South Florida, 140 Seventh Avenue South, MSL 119, St. Petersburg, FL 33701, USA. (quinn@seas.marine.usf.edu)

F. W. Taylor, Institute for Geophysics, University of Texas at Austin, John A. and Katherine G. Jackson School of Geosciences, 4412 Spicewood Springs Road, Austin, TX 78759-8500, USA. (fred@ig.utexas.edu)